Frequency analysis of reinforced concrete structures subjected to accidental impacts

Christophe Rouzaud, Fabrice Gatuingt, Olivier Dorival, Guillaume Hervé, Nadim Moussallam

Frequency analysis of reinforced concrete structures subjected to accidental impacts

Christophe Rouzaud[1,2,3], Fabrice Gatuingt[1], Olivier Dorival[4], Guillaume Hervé[2], Nadim Moussallam[3]

[1]LMT-Cachan, ENS Cachan/UPMC/CNRS/Paris 6 University, 61, avenue du Président Wilson, Cachan 94235, France, {christophe.rouzaud, fabrice.gatuingt, olivier.dorival}@ens-cachan.fr
[2]Université Paris-Est, Institut de Recherche en Constructibilité, ESTP, 28, Avenue du Président Wilson, F-94230, Cachan, France, {crouzaud, gherve}@adm.estp.fr
[3]AREVA, 10, Rue Juliette Récamier Lyon 69006, France, nadim.moussallam@areva.com
[4]Université de Toulouse; Institut Clément Ader (ICA); INSA, UPS, Mines Albi, ISAE 135 av. de Rangueil, 31077 Toulouse cedex, Olivier.Dorival@isae.fr

Introduction

If an industrial structure is designed to withstand a direct commercial aircraft impact, the vibrations induced by such a shock would propagate throughout the walls and slabs of this structure. These vibrations might result in significant dynamic excitation of the internal equipments. If these equipments are needed after the impact, typically to bring the industrial facility to a safe state, they must be designed to withstand this dynamic excitation. It is therefore necessary to determine the type and amplitude of the vibrations induced by the aircraft impact on the structure. This determination is usually performed by dynamic analyses studies. From the structure point of view, the commercial aircraft impact results in a bending problem. This phenomenon induces the formation of a localized non-linear area around the impact zone, where cracks are formed into the concrete and the reinforcement bars yield. Far from the impact zone, where vibrations levels are seeked for the design of equipments, it can be considered that the structure remains essentially elastic.

The structural dynamic response to an aircraft impact can be determined by using classical finite element method (FEM) associated with explicit numerical schemes. This method is relatively costly in terms of calculation time. This cost is due to the fact that FEM calculations must be carried out with a mesh refined enough to take into account the all the wavelengths of the induced motions. The cutoff frequency for this type of loading is typically within the 50 to 100 Hz range, which would be referred to as the high frequency range [HER13]. The use of a refined mesh then leads to the need for a refined time discretization. As a consequence, the high frequency range is often less precisely represented than the low frequency content.

The purpose of our study is to develop new ways for calculating the induced vibrations in reinforced concrete structures submitted to a commercial aircraft impact. The paper is structured as follows: Section 1 presents the description of the strategy used; Section 2 describes an example case and the input signal applied to it; Section 3 illustrates the determination of the non-linear area through a FE calculation; the Section 4 explains the VTCR method and shows its application on the industrial structure; finally, conclusions and perspectives are drawn in Section 5.

1 Description of the strategy

To solve our problem of shock induced vibrations in a reinforced concrete structure and assuming that the structure is appropriately sized to withstand an aircraft impact, the strategy implemented is as follows (see Figure 1).

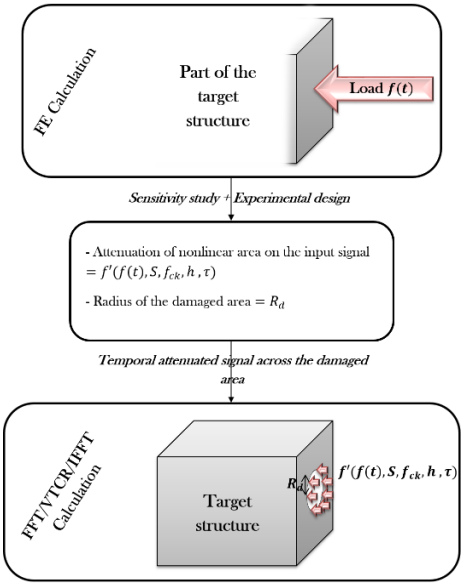

Figure 1. Global calculation strategy.

The aircraft is replaced by an equivalent force-time function. This equivalent load is applied on a finite element model of a part of the target structure and its nonlinear response is calculated by finite element method. This calculation allows us to determine the radius of the nonlinear area and the induced attenuation of the input signal at the periphery of this area.

The temporal attenuated signal can then be applied at the boundary of the above mentioned area on a linear model of the complete structure. The structure response is obtained by a simulation with the VTCR (Variational Theory of Complex Rays). This calculation requires a transformation from time to frequency domain that is achieved by FFT (Fast Fourier Transform). After solving the problem in the frequency domain, a time recomposition is performed by IFFT (Inverse Fast Fourier Transform). The VTCR ([LAD01]) ensures an efficient calculation of the response of the structure in frequency domain. The VTCR uses two-scale shape functions which satisfy exactly the dynamic equation and the constitutive relation within each substructure. The solution is searched as a combination of propagative and evanescent waves.

2 Description of an example case

2.1 Description of the structure

Let us consider a concrete structure where the mechanical properties of concrete are extracted from the rules of Eurocode 2:

- concrete B30 = 30 MPa,
- Young's modulus = 34 GPa,
- Poisson's ratio = 0.2,
- mass density = 2500 kg/m^3,
- damping coefficient= 0.07.

In this study, a hysteretic damping is used. The structure (Figure 2) is entirely 1 m constituted of 1m thick shells. It comprises four peripheral square building and one central cylindrical building with a dome shaped roof.

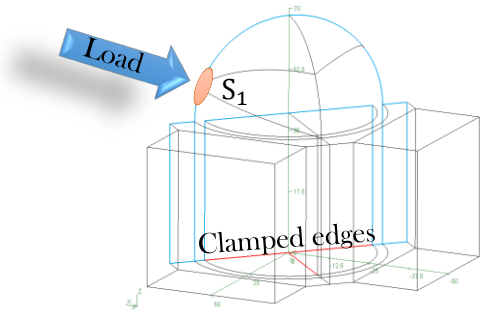

Figure 2. Geometry of the numerical example.

The structure is subjected to a normal impact applied at the surface S_1 of the dome. This impact produces localized damages on this part of the structure. A detailed in the previous Section, the radius of the non-linearity area will be calculated in a first step by the FEM and the temporal attenuated signal in displacement across the damaged area will be applied on the rest of the structure. We consider the load at S_1 as a force of an aircraft impact calculated by a modification of Riera's analytical approach. This approach will be presented in the section (2.2).

2.2 Description of the input signal

Nowadays, transient FE models are often used to evaluate the load produced by an aircraft crash impact over a structure. Both target and missile are commonly represented in these models. The meshing should therefore be very fine, with an associated high resolution cost. The aim of this section is to expose the results of an alternative modeling, which uses a force of impact signal calculated by a modification of Riera's analytical approach [RIE80] instead of using a model for the entire plane.

2.2.1 Progressive crushing: Stationary hinges model

In real tests [ABR86] carried out with metallic pipe sections impacted over concrete walls, the resultant deformation of the missile after the impact could be described as series of folds formed all along the impacted section.

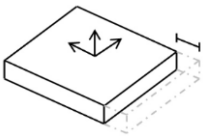

(a) Membrane energy E_m

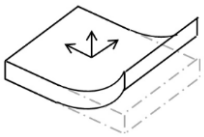

(b) Bending energy E_b

Figure 3. Modes of energy dissipation in SHELL elements.

Apart from the initial peak, governed by an elastic-plastic buckling, the load displacement behavior exhibits a repeated peaks pattern where each pair of peaks is associated with the development of one full buckle. Normally, the buckles develop sequentially from one end of the tube so that the phenomenon is known as a progressive crushing (see Figure 4).

(a) Crushed circular tube test specimens [ABR86]

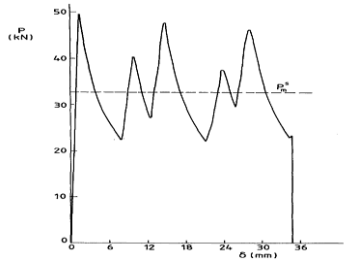

(b) Static axial load versus crushing distance for test specimen [ABR86]

Figure 4. Modes of energy dissipation in SHELL elements.

The original analysis developed by Alexander [ALE60] was motivated by a specific need for predicting energy absorption of dropped objects in nuclear reactors application. In this context, a technique is proposed for estimating the global parameters of the crushing process related directly with the crushing force and the energy absorbed by compressed members. The model starts from two straight elements, ABC and CD of length $2H$ each, which are connected by stationary plastic hinges. The wavelength H is an unknown parameter which will be found in the course of the analysis. Following Alexander, it is postulated that the half length of the folding wave adjusts itself so as to minimize the mean crushing force. Through the folding process, the deflection of the first deformed element, ABC, with respect to the horizontal is denoted by α while the second element, CD follows an angle β. Due to the current geometry, α and β are related by:

$$cos\beta = cos\alpha - cos\alpha_0 \quad (1)$$

where $cos\alpha_0 = m$ and m is the eccentricity of the folding.

The eccentricity of the folding process is conveniently described by the parameter m. Form $m = 0.5$ the folds extend the same distance on both sides of the initial radius. A fully external folding corresponds to $m = 0$ while an internal folding is obtained by setting $m = 1$. The eccentricity is a parameter which must be assumed.

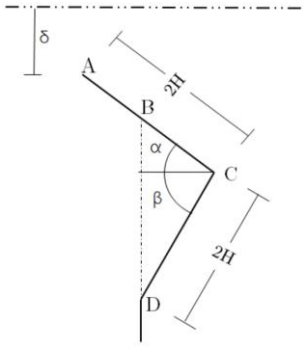

Figure 5. Diagram of virtual displacement in the walls of the element.

and associated to the longitudinal deformation by the expression:

$$\delta = 2H\,(1 + sin\alpha_0 - sin\alpha - sin\beta) \quad (2)$$

This model discretizes the pipe into series of plates which contribution will be integrated to get the one of the complete pipe section. The crushing phenomena is presented in two phases of folding process:

• *Phase 1 Beginning of the folding process.*

In this step we calculate the amount of energy which is necessary for reaching a slope of angle α_0 starting from a straight section by developing a unique plastic hinge. The deformation continues decreasing the value of α Equation 2, remaining β and pursuing the total amount of energy Equation 3 necessary to make α equal to $\pi/2$.

$$\dot{E}_m^I + \dot{E}_b^I = -4\pi N_0 H^2 sin\alpha\dot{\alpha} + 4\pi R_0 M_0(|\dot{\alpha}|) \quad (3)$$

• *Phase 2 Iterative folding process.*

Once the value α_0 has been reached, it begins the second phase which is characterized by the presence of two plastic hinges.

The longitudinal deformation continues just to reach an angle α equal to 0 that points out the end of fold and the beginning of the next one; the next fold will start retaking the last value of β as the new value of α and taking β from the very beginning of a straight section ($\pi/2$). This process repeatedly continues until the end of the longitudinal section.

$$\dot{E}_m^{II} + \dot{E}_b^{II} = -8\pi N_0 H^2 sin\alpha\dot{\alpha} + 4\pi R_0 M_0(|\dot{\alpha}| + |\dot{\beta}|) \quad (4)$$

With these two equations, Equation 3 and Equation 4, and using the principle of virtual velocities, the load-shortening behavior, equivalent to the crushing force, is given by:

$$P(\dot{\delta}) = \dot{E}_m + \dot{E}_b \quad (5)$$

The principal limitation lies in the consideration that a cylindrical shell is deformed into a flat of annular discs meaning that the entire length is available for crushing, which is inaccurate. Despite its limitations, the assumption that one folding wave forms at a time has remained unchallenged.

2.2.2 **Modified Riera: Pearl's** algorithm for aircraft crash including the progressive crushing effects

The approach made by Riera considers a simplified distribution of the crushing force along the body of the aircraft, which results in a regular signal of impact force, without peaks.

The signal obtained from finite element models of aircraft, found in the literature, several peaks. These peaks in the impact force functions could be explained by two main sources:

- flexural behavior of the type and the size of the elements used for the aircraft model (usually SHELL element type),
- progressive crushing of the plane's elements (characteristic of the impact on pipes).

With the aim of having a better representation of the crushing phenomenon, it was decided to include the folding effect in the Riera's analysis of aircraft by using the methodology proposed by Alexander. The following hypotheses were considered.

- the crushing-pipe behavior is presented only in the fuselage; the rest of the plane is treated according to the Riera's method,
- the fuselage is represented by an equivalent pipe section (based on the Riera's crushing force and the average radius of the fuselage),
- the folds are formed one by one along the section there is no presence of the first phase of the Alexander's folding methodology due to the presence of the nose of the aircraft which will produce at the impact a deformation of the fuselage.

The target load curve is plotted in the Figure 6. In order to carry out this example without impairing any confidentiality aspects the values of the impact forces have been divided by the peak value of the signal. Thus the maximal value is 1 and no existing curve is especially pointed out.

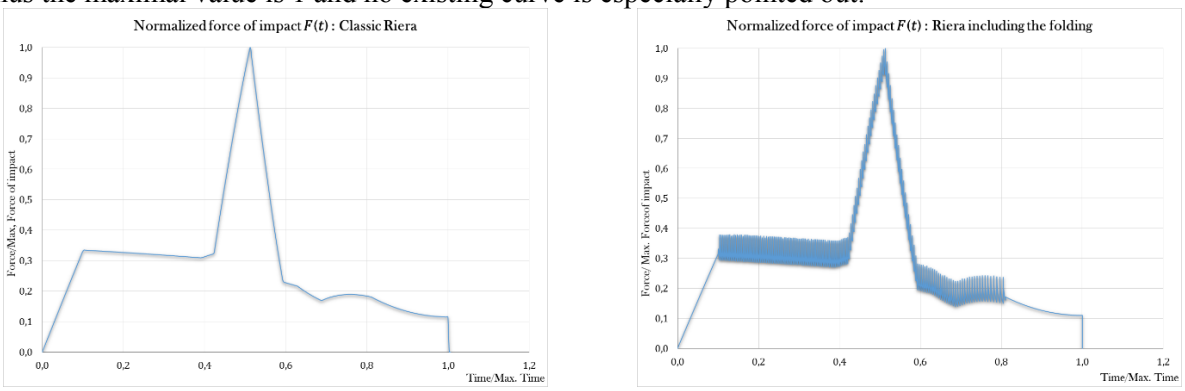

(a) Classic Riera (b) Riera including the effect of folding pipes

Figure 6. Force of impact $F(t)$ calculated for a generic airplane.

As we can notice, the incorporation of the folding effect along the fuselage brings a signal in the frequency domain which differs, over 30 Hz, from 1% to 137% with respect to the classic Riera.

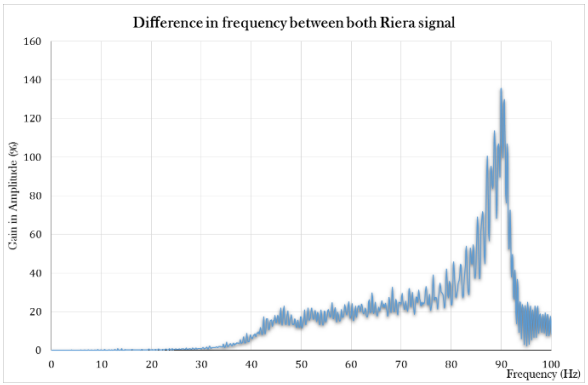

Figure 7. Difference in frequency in percentage between classical Riera's signal and crushing signal.

3 Determination of the non-linear area

In this work we employ LS-Dyna [LSDYNA] for calculation, with Lagrangian finite elements and explicit time integration. Given the initial geometry, we decided to focus our study on the dome of the structure and, the boundary conditions are defined as constrained in displacements. The dome was modeled by shell elements, for a low computation cost model and for an easier transfer of the result to the linear full structure model. The constitutive law of concrete *Mat_Concrete_EC2*, implemented in LS-Dyna, was used for the elements.

A loading history corresponding to the modified Riera's signal see in Figure 6b is taken into account, this force is applied over a period of 1 s. The load is applied on a surface of 12 m^2. This area corresponds to the fuselage of the aircraft. The concrete cover will remain constant and equal to 10 cm to the under and upper side. The material model *Mat_Concrete_EC2* ([HAL06]) is associated with multi-sheets model to define different layers in the thickness of the wall. This model is used for structural elements (shells and beams). It can either represent plain concrete only, reinforcing steel only, or a smeared combination of concrete and reinforcement. The model includes concrete cracking in tension, concrete crushing in compression, and reinforcement yield, hardening and failure. Material data and equations governing the concrete and reinforcement behavior (including thermal properties) are taken from [EUR05]. The dome meshing is constructed so as to be able to represent up to a frequency of 100 Hz, in accordance with the engineering rule of 10 elements per wavelength. So the mesh size is equal to 50 cm.

Finally, this non-linear calculation allows us to obtain a radius of the damaged area of 10 m and a displacement at the ends of this area shown in Figure 8.

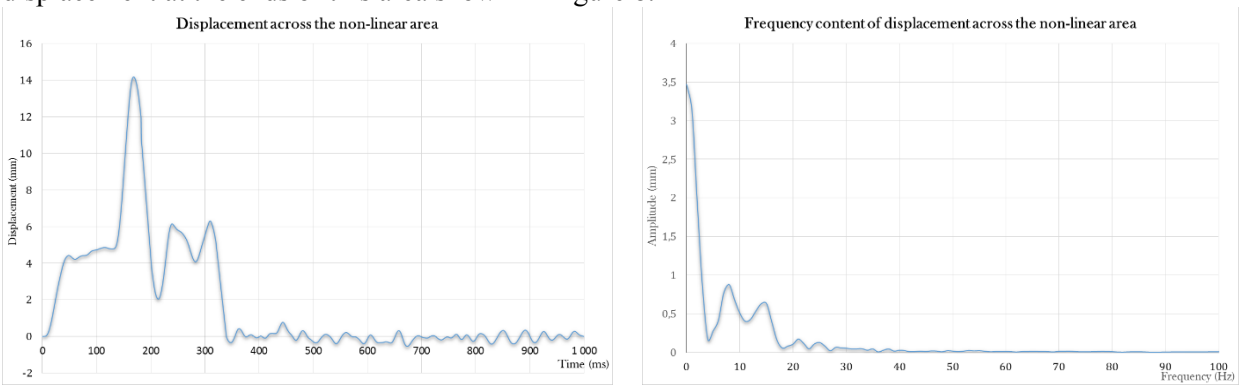

Figure 8. Displacement time history across the non-linear area (left) and associated frequency content (right).

In the next step, this displacement is applied to the linear model representing the rest of the structure.

4 Frequency analysis

4.1 Description of the variational Theory of complex rays (VTCR)

This work, which uses new computational strategies in dynamics, provides an answer for the steady state of the solution. The problem is solved in the frequency domain. One needs to solve a forced vibration problem over a frequency range which includes the low- and medium-frequency ranges ([OHA98]). The low-frequency and medium-frequency ranges are handled using the Variational Theory of Complex Rays (VTCR) [LAD01].

4.1.1 The reference problem for an assembly of n substructures

We consider the case of homogeneous Kirchhoff-Love's thin shells which vibrate at a pulsation ω. The thickness is h_i and the density ρ_i. The displacement $\underline{U_i}$ of the average surface can be formulated as:

$$\begin{aligned} \underline{U_i}(x,y,z) &= \underline{u_i}(x,y) + w_i(x,y)\underline{e_3}_i + z\underline{\theta_i} \\ \underline{\theta_i}(x,y) &= -\underline{grad} w_i(x,y) - \underline{\underline{B_i}}\,\underline{u_i}(x,y) \end{aligned} \tag{6}$$

where $\underline{u_i}$ is the in plane displacement of the average surface, w_i is the out of plane displacement and $\underline{\underline{B_i}}$ the curvature tensor. The average surface of the shell is defined by two independent parameters α_i and β_i. The position of a point on the medium surface is defined by the position vector $\underline{r_i}(\alpha_i, \beta_i)$ (see Figure 9).

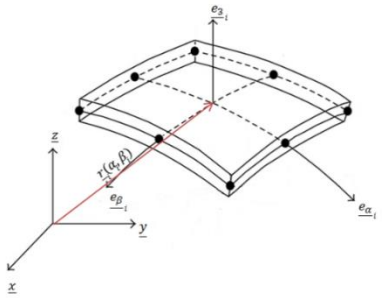

Figure 9. Geometry of a shell Ω_i.

Let n shells Ω_i, with a common border Γ. The actions of the environment are modeled on Ω_i by imposing displacement on $\partial_w \Omega_i$ and $\partial_{\underline{u}} \Omega_i$, rotations on $\partial_{w,\underline{n}} \Omega_i$, line stresses on $\partial_K \Omega_i$ and $\partial_{\underline{N}} \Omega_i$, and line momentum on $\partial_M \Omega_i$. Figure 10 shows the actions of the environment between the field Ω_i and Ω_j.

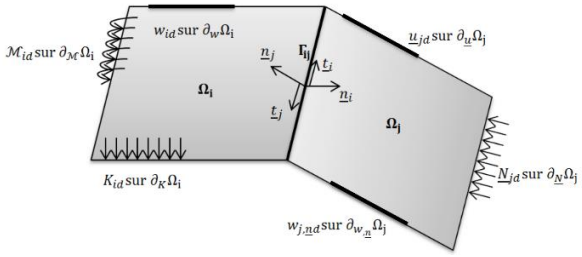

Figure 10. The reference problem.

The reference problem to be solved is define in [ROU13].

4.1.2 The variational formulation associated to the VTCR

The 1st ingredient of VTCR is a global weak formulation of the boundary conditions in terms of both displacements and forces. The variational formulation can be expressed as: find $\left(\underline{u_i}, w_i, K_i, \underline{\underline{N_i}}, \underline{\underline{M_i}}\right) = \left(\underline{U_i}, \underline{\underline{\sigma_i}}\right) \in S_{ad,i}$ such as:

$$\mathcal{A}\left(\begin{vmatrix} s_1 \\ \dots \\ s_n \end{vmatrix}, \begin{vmatrix} \delta s_1 \\ \dots \\ \delta s_n \end{vmatrix}\right) = \mathcal{L}\left(\begin{vmatrix} \delta s_1 \\ \dots \\ \delta s_n \end{vmatrix}\right) \tag{7}$$

with the following general form:

$$\mathcal{A}\left(\begin{vmatrix} s_1 \\ \dots \\ s_n \end{vmatrix}, \begin{vmatrix} \delta s_1 \\ \dots \\ \delta s_n \end{vmatrix}\right) = \mathcal{R}e\left\{-i\omega\left[\sum_{i=1}^{n}\int_{\partial_{\underline{u}}\Omega_i}\delta\underline{\underline{\sigma}}_i\underline{n}_i.\underline{U}_i^*d\mathcal{S}+\sum_{i=1}^{n}\int_{\partial_{\underline{F}}\Omega_i}\underline{\underline{\sigma}}_i\underline{n}_i.\delta\underline{U}_i^*d\mathcal{S}\right.\right.$$
$$\left.\left.+\int_{\Gamma_{ij}}\begin{Bmatrix}\frac{n-1}{n}\sum_{i=1}^{n}\left(\delta\underline{\underline{\sigma}}_i\underline{n}_i\right).\left(\underline{U}_i\right)^*+\frac{1}{n}\sum_{i\neq j}\left(\delta\underline{\underline{\sigma}}_i\underline{n}_i\right).\left(\underline{U}_j\right)^* \\ +\frac{1}{n}\sum_{i=1}^{n}\left(\underline{\underline{\sigma}}_i\underline{n}_i\right).\left(\delta\underline{U}_i\right)^*-\frac{1}{n}\sum_{i\neq j}\left(\underline{\underline{\sigma}}_i\underline{n}_i\right).\left(\delta\underline{U}_j\right)^*\end{Bmatrix}d\mathcal{S}\right]\right\} \quad (8)$$

$$\mathcal{L}\left(\begin{vmatrix} \delta s_1 \\ \dots \\ \delta s_n \end{vmatrix}\right) = \mathcal{R}e\left\{-i\omega\left[\sum_{i=1}^{n}\int_{\partial_{\underline{u}}\Omega_i}\delta\underline{\underline{\sigma}}_i\underline{n}_i.\underline{U}_{id}^*d\mathcal{S}+\sum_{i=1}^{n}\int_{\partial_{\underline{F}}\Omega_i}\underline{F}_{id}.\delta\underline{U}_i^*d\mathcal{S}\right]\right\} \quad (9)$$

where:

- the integral part on $\partial_{\underline{u}}\Omega_i$ check on average the imposed displacements on Ω_i,
- the integral part on $\partial_{\underline{F}}\Omega_i$ satisfy the imposed stresses on Ω_i,
- the integral part Γ_{ij} on satisfy the transmission conditions on the boundary Γ_{ij}.

$\mathcal{R}e$ designates the real part of a quantity and $*$ the conjugate part. Spaces $S_{ad,i}^0$ are the space of admissible fields associated with homogeneous conditions on the structure i: $\underline{f}_{d,i}=0 \qquad i=1,\dots,n$. In our case, $S_{ad,i}^0 \equiv S_{ad,i} \qquad i=1,\dots,n$.

It is based on a priori independent approximations within the substructures. The constitutive relation (Equation 8) and dynamic equilibrium equation (Equation 10) are exactly satisfied for each substructures Ω_i to form the corresponding subspace $S_{ad,i}$.

It is easy to prove that the variational form is equivalent to the reference problem, provided that:

- the reference problem has a solution,
- the Hooke's operator $\underline{\underline{\underline{\underline{K}}}}_{CP_i}$ is positive definite,
- the damping coefficients are such that $\eta_i > 0$,

The rigid body movements are blocked provided that $\omega > 0$.

4.1.3 Derivations of two-scale shape functions

The VTCR uses a two scale approximation of $\left(\underline{U}_i^h, \underline{\underline{\sigma}}_i^h\right)$, that exhibits a strong mechanical meaning because they satisfy the constitutive and dynamic equilibrium equation. The solution is assumed to be properly described locally as the superposition of an infinite number of local vibration modes which can be written in the following manner:

$$\begin{aligned}\underline{U}_i\left(\underline{X}_i,\underline{Y}_i,\underline{P}_i\right) &= \underline{U_n}_i\left(\underline{P}_i\right).e^{\underline{P}_i.\underline{X}_i} \quad \text{on } \Omega_i \\ \underline{\underline{\sigma}}_i\left(\underline{X}_i,\underline{Y}_i,\underline{P}_i\right) &= \underline{\underline{C_n}}_i\left(\underline{P}_i\right).e^{\underline{P}_i.\underline{X}_i} \quad \text{on } \Omega_i\end{aligned} \quad (10)$$

where $\underline{X}_i$ represent the position vector. $\underline{P}_i$ is the complex wave vector associated with the vibration rays in the plane of the shell. In order for these local modes $\left(\underline{U}_i, \underline{\underline{\sigma}}_i\right)$ to be admissible, they must be in $S_{ad,i}$ and satisfy the constitutive and dynamic equilibrium equation. The mechanical waves can be divided into three families (see Figure 11): the P waves (Primary), SH (Secondary Horizontal) and SV (Secondary Vertical). We can identify two types of mechanical waves which can describe the membrane effect, the P waves for the pressure effects and the SH waves for shear effects.

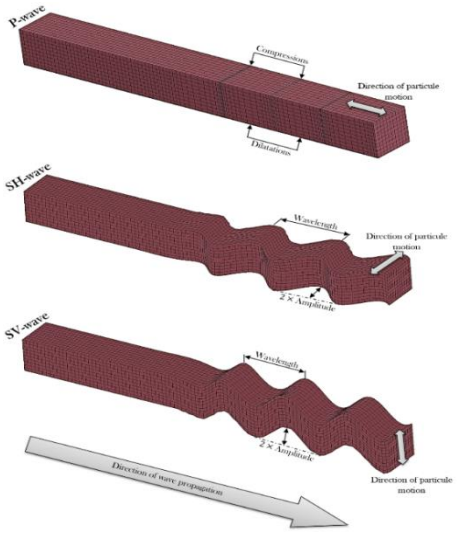

Figure 11. Three families of mechanical waves.

4.1.4 The discretized problem

The displacement of any point of the substructure is generated by a basis of admissible complex rays. The unknown is the generalized amplitude $\underline{U}_i^h(\underline{X}_i, \underline{P}_i)$ of the basis (an n^{th}-order polynomial in $\underline{X}_i$ and a large-wavelength quantity). Accounting for all the directions of propagation φ_i and θ_i in the circle C_i leads to an integral over C_i. This integral takes the form:

- bending displacement:

$$w_i^h(\underline{x}_i) = \int_{\varphi_i \varepsilon C_i} W_i^h(\varphi_i) e^{\underline{P}_{bi}(\varphi_i).\underline{x}_i} d\varphi_i \qquad (11)$$

with $\underline{P}_{bi}$ determined by the dispersion relation from the solution of Equation 11.

- membrane displacement:

$$\underline{u}^h(\underline{x}_i) = \int_{\theta_i \varepsilon C_i} \underline{u_0}_i^h(\theta_i).\, e^{\underline{P}_{mi}(\theta_i).\underline{x}_i} d\theta_i \qquad (12)$$

with $\underline{P}_{mi}$ determined by the dispersion relation from the solution of Equation 11.

Let us note that admissible space $S_{ad,i}$ is of infinite dimension since, for instance for interior modes, all directions of propagation $\underline{P}_i$are taken into account. To end up with a finite dimension problem that can be solved numerically, one need to discretize $S_{ad,i}$ into a finite dimension space $S_{ad,i}^h$. The integral in Equation 16 and Equation 17 can be discretized as Dirac functions and we can consider the approximate amplitude $\underline{U}^h\left(\underline{P}_i(\varphi_i)\right)$. The advantage of this choice is that all directions of propagation are still represented in the discretized space, though with an approximation on their amplitude (see Figure 12).

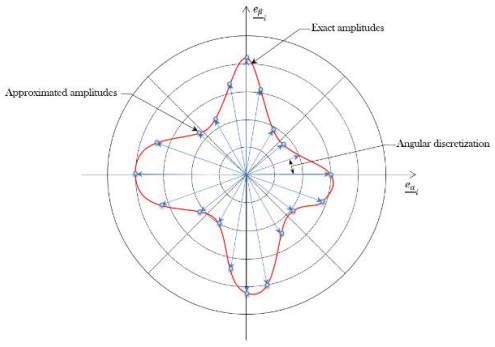

Figure 12. The discretized amplitudes.

This discretization is related to several parameters, it is thus difficult to define it analytically. An iterative approach, based on a heuristic criterion, is then used to reduce errors and verify that the boundaries conditions are respected. A number of waves between 20 and 100 is generally sufficient.

4.2 VTCR results

The determination of the parameters controlling the nonlinear area localized at the impact surface allows us to study the rest of the structure. For this we use the frequency domain through the VTCR method described in paragraph 4.1. We apply to the displacement across this area defined in the Figure 8. To study the response of the VTCR we put 5 points (P_1, P_2, P_3, P_4 and P_5) on the structure where we will reconstruct the resulting displacement time histories. These points are illustrated in Figure 13.

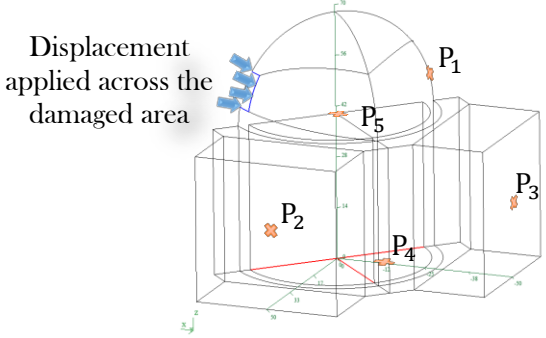

Figure 13. Geometry of the linear part of the structure.

Three hundred rays per substructure are sufficient to properly represent the frequency response. The Table 1 shows the solution obtained for four example frequencies. The boundary conditions are in a good adequacy. This is clearly observable where the load is applied and on the structure supports.

Table 1. VTCR solution of numerical example.

	Max/per substructures: 40 interior modes, 4*40 edge modes, 50 pressure modes and 50 shear modes	
	10 Hz	25 Hz
resultant displacement (mm)	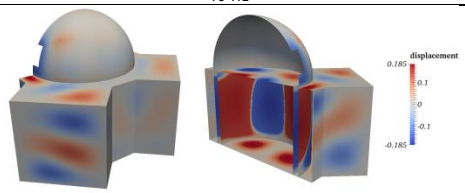	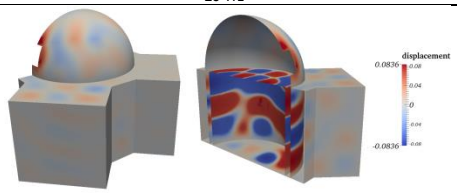
	50 Hz	100 Hz
resultant displacement (mm)	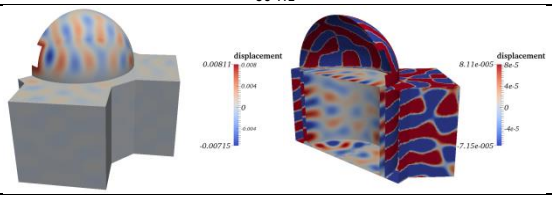	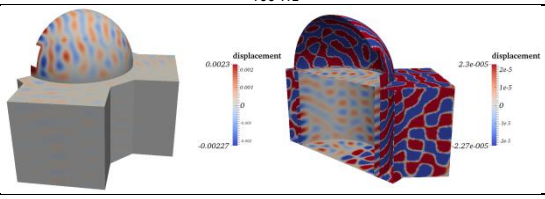

Following the VTCR calculation we can recover the amplitude and the phase of each point of the structure in each frequency and thus reconstruct the time response by IFFT. For the selected point P_4, the following displacements (see Figure 14) and response spectrum in out-of-plane acceleration (see in Figure 15) were obtained. To validate the results obtained with the VTCR we compare them with those obtained by a FEM and calculated with CAST3M [CAST3M]. In this comparison, and in order to show the influence of mesh size on the level of accuracy of results, we use two meshes. An initial coarse mesh define as having a mesh size of 2 m, which is composed of 15,000 degrees of freedom. If we refer to the engineering rule of 10 elements per wavelength, this mesh can represent a frequency range limited to 25 Hz. The second mesh is refined and define from a mesh size of 0.5 m or so nearly 400,000 degrees of freedom and a frequency range limited to 100 Hz.

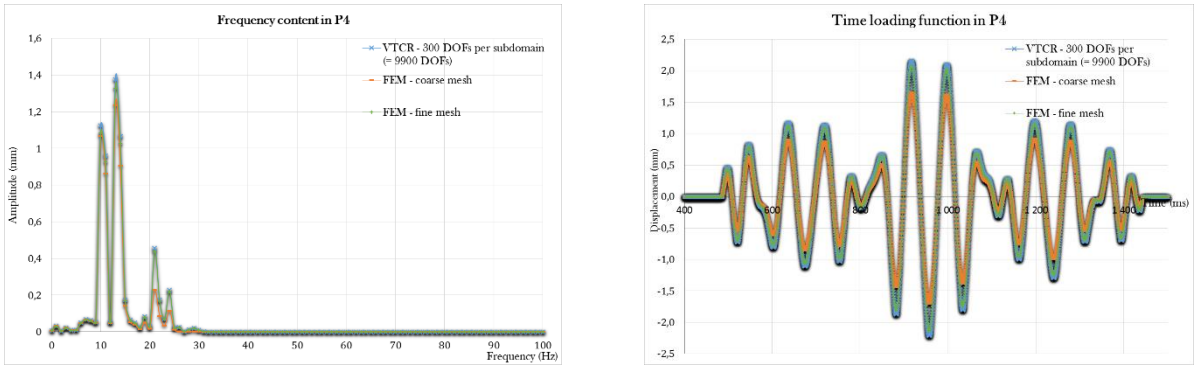

Figure 14. Displacement amplitude (left) in P_4 and the associated inverse Fourier transform (right), out-of-plane displacement w_{P_4}.

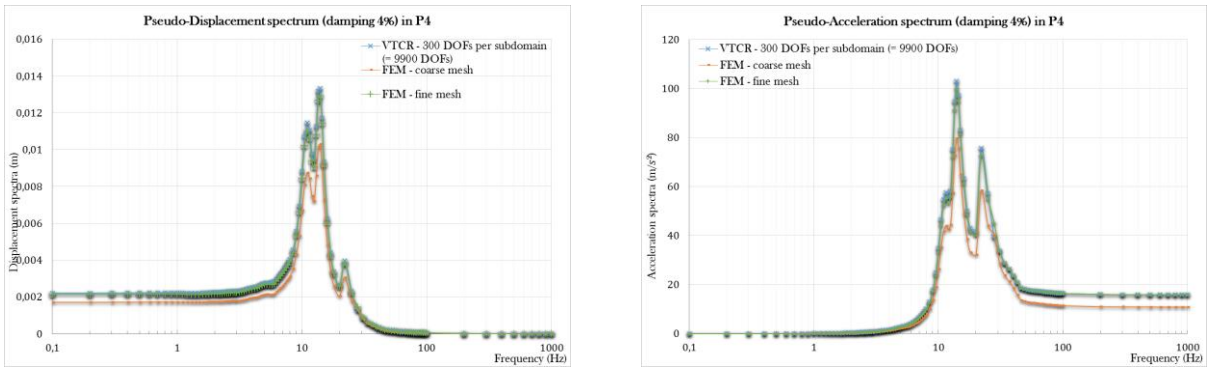

Figure 15. Out-of-plane pseudo-displacement (left) and pseudo-acceleration (right) response spectrum in P_4.

We can then conclude from these results two important points. First, we note that with the VTCR resolution we get, with less degrees of freedom, similar results to those obtained in the case of a fine FEM calculation. The second point is on the FEM mesh size. Indeed, one can realize that, with the engineering rule of 10 elements per wavelength, the results for the upper limit of the frequency range are not in a god adequacy. We will recommend to choose between 15 and 20 elements per wavelength.
Figure 16 shows the difference in CPU time between the resolution with VTCR and the resolution with CAST3M ([CAST3M]) for this problem. In this figure, the red curve shows different points representing the time required for calculating the solution by increments of $10Hz$. The blue curve provides the computation time for different mesh densities. This density must be thin enough to properly represent the solution.

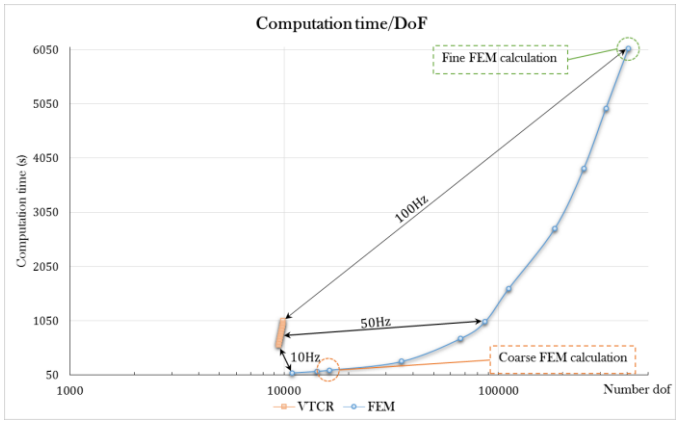

Figure 16. Comparison between VTCR and CAST3M in terms of computation time.

Conclusions

A methodology to determine the aircraft impact induced vibrations in a structure was presented. It is based on the use of a preliminary nonlinear local FE model and of a subsequent linear representation of the complete structure using the VTCR theory. The methodology was successfully applied on an example case of a civil engineering structure.

The results were shown to be in perfect accordance with the one produced by a standard FE model, within the frequency range of validity of such FE model. Above this frequency range, the VTRC methodology is still able to produce quick and accurate results, where the use of a FE model would be unaffordable in terms of calculation costs. This superiority is due to the much reduced number of degrees of freedom needed for reaching a same level of accuracy. Especially a focus can be easily made on dedicated and selected frequencies of interest.

It is expected that the tools and methods described here will find a use in the nuclear industry, among others, where the complexity of the structures make the realization of an accurate FE model tedious and costly.

References

[ABR86] Abramowicz W., and Jones N., *«Dynamic progressive buckling of circular and square tubes»,* International Journal of Impact Engineering, Vol. 4 No. 4, pp 243-270, 1986.

[AIE12] AIEA, *«Safety Assessment of NPP Structures against Human Induced External Events»,* IAEA Safety Report Series, DD1086 Draft, Rev.: R1- 1, 2012.

[ALE60] Alexander J.M., *«An approximate analysis of the collapse of thin cylindrical shells under axial loading »,* Q.J. Mech. Appl. Math., No. 13, pp 10-15, 1960.

[CAST3M] *http://www-cast3m.cea.fr/.*

[DOR08] Dorival O., Rouch P. and Allix O., *«A substructured Trefftz method for updating joint models in the medium-frequency range»*, Computational Mechanics, Vol. 42 No. 3, pp 381-394, 2008.

[EUR05] EC2, *«Eurocode 2 - Calcul des structures en béton - Partie 1-2 : Calcul du comportement au feu»*, NF EN 1992-1-1, 2005.

[HAL06] Hallquist, JO, *«LS-DYNA theory manual»*, Livermore Software Technology Corporation, 2006.

[HER13] Hervé G., Rouzaud C., Barré F. and Secourgeon E., *«Optimizing the analysis of airplane crash induced spectra by means of generic airplane methodology»*, SMIRT-22, 2013.

[LAD01] Ladeveze P., Arnaud L., Rouch P. and Blanze C., *«The variational theory of complex rays for the calculation of medium-frequency vibrations»*, Engineering Computations, Vol. 18, pp 193-214, 2001.

[LAR80] Laroze S. ., *«Résistance des matériaux et des structures. Tome 1: milieux continus, plaques et coques»*, Eyrolles, Paris, 1980.

[LSDYNA] *http://www.lstc.com /.*

[OHA98] Ohayon R. and Soize C. ., *«Structural acoustics and vibrations»*, Academic Press, 1998.

[RIE80] Riera J., *«A critical reappraisal of nuclear power plant safety against accidental aircraft impact»,* Nuclear Engineering and Design, 57, 1980.

[ROU13] Rouzaud C., Gatuingt F., Dorival O., Hervé G. and Moussallam N., *«A new way for the study of the shaking of reinforced concrete structures»,* TINCE, 2013.

[VLA13] Vlaski V., Gatuingt F., Dorival O., Hervé G. and Moussallam N., *«Reduction of External Hazard (Fast Impact) Induced Vibrations»,* TINCE, 2013.